Evaluation on Implementing an Active Braking System in Wheelchair Rear-Mounted Power-Assisted Device

Evaluation on implementing an active braking system in wheelchair rear-mounted power-assisted device

Valerio Cornagliotto[1], Flaminia Perino[1], Laura Gastaldi[1] and Stefano Pastorelli[1]

[1]Dept. of Mechanical and Aerospace Engineering, Politecnico di Torino, Turin, Italy
valerio.cornagliotto@polito.it

Abstract. Power-Assisted Devices (PADs) for wheelchairs are becoming popular tools to enhance propulsion capabilities and to assist wheelchair users to perform daily activities. PADs include Pushrim Activated Power-Assisted Wheelchairs, joy-stick-driven wheels, front-end attachments, and rear-end attachments. Considering the latest, they are not equipped with any active braking system. This could affect the handling of the wheelchair and introduce safety concerns.

The paper aims to assess the performance of a rear add-on during driving and braking conditions, and to investigate the implementation and effectiveness of a servo braking system. A dynamic multibody model of a wheelchair has been developed and the dynamic of the system has been analyzed. To enhance the braking effectiveness, an additional preload torque between the wheelchair and the device has been modelled. Simulations have been performed for different braking torques. The results show that the introduction of a mounting preload positively affects the braking effectiveness, and it assists the user to perform part of the braking action.

Keywords: Add-on, PAPAW, braking system, power-assisted devices

1 Introduction

Many manual wheelchair (MWC) users might have to struggle to move and to accomplish everyday activities. The difficulty could be due to reduced physical ability, upper body weakness, pain, injuries, or fatigue due to wheelchair propulsion for a prolonged time. Facilitating wheelchair users' mobility is in line with the aim of the third sustainable development goal (SDG3) - healthy lives and promotion of well being. Active assistive devices to reduce wheelchair users' effort have been developed [1]. Previous studies demonstrated that power-assisted devices (PADs) positively influenced the propulsion capabilities, reducing the biomechanical and physiological effort associated with manual wheelchair self-propulsion [2]–[4] and improved mobility [5]. Currently, different kinds of PADs are commercially available. PADs include Pushrim Activated Power-assisted Wheelchairs (PAPAWs), joystick-driven wheels, front-end attachments, and rear-end attachments. PAPAWs consist of motorized wheels which provide a propelling torque proportional to the torque exerted on pushrims by the user (e.g., Servo®, Twion®, e-motion®). Joystick controlled wheels (e.g., e-fix®, Solo®), which

might be mounted on a personal wheelchair, allow the user to control the MWC motion through a joystick mounted on the armrest. Front-end add-on devices are attached to the front of a MWC lifting the caster wheels off the ground thus converting the MWC into a powered tricycle (e.g., Batec®, etc). At last, the rear-mounted devices consist of an additional powered wheel, attached to the MWC wheel axis, that provides longitudinal thrust. Rear-mounted devices are generally controlled through a wristband or knobs (e.g., SmartDrive MX®, SmoovONE®, YOMPER®).

In previous studies, the characteristics and the users' perception of some PADs have been investigated [6]–[12]. The mounting procedure of the front-end devices turned out to be easier than the others PADs, on the other hand, the PAPAW or rear-mounted devices footprint is smaller [8]. Moreover, rear add-on devices are lighter than the other solutions taken into account [6]. Some differences also emerged concerning the operation and control of the devices. The PAPAWs usually detect the user intention through the evaluation of the torque exerted on the pushrim. Then, the device provides the additional torque proportional to the one exerted by the user at each actuated wheel. Thus, the user perceives a lower effort to thrust the wheelchair. The user has to repeat the push on the handrims to continue the movement. With front-end attachments, the input is given by a handlebar, similarly to a scooter or tricycle. Rear-mounted solutions are controlled in different ways, depending on the model and the selected driving mode. Some devices adopt a wristband or a smartwatch as input interface, others detect the user's intention to activate the device monitoring the add-on motor motion. In all the rear-mounted solutions a velocity control is implemented, hence the devices sustain the propulsion at a given speed until the user provides an input to change the speed or arrest the device. As regards the braking function, each PAD model requires a different user's input. In PAPAWs and front-mounted solutions, the device itself provides an active action (mechanical or electrical), and the user only needs to give the braking command as input to the device. In PAPAWs, since the torque supplied by the device is proportional to the torque provided by the user, when the hand exerts resistance torque, the device applies a braking torque. In the front-end attachments, the braking input is given directly through the handlebar brake which controls a mechanical braking system. In rear add-ons there is no active assisted braking. The user who intends to stop the wheelchair has to switch off the device and exert theirself the braking force directly on the pushrims. Unlike PAPAWs, the rear-mounted device is not controlled by sensors on the handrims; therefore, the user is requested to switch off the device by using a button or performing different gesture with the wristband. Indeed, some devices detect the user intention by monitoring the current absorbed by the motor. Since the motor doesn't exert an active braking torque, the user has to exert theirself the whole amount of force required to stop the wheelchair. The physical effort required to handle the wheelchair equipped with rear-mounted devices has been investigated in [8] and [9]. It turned out that users suffered from hands pain due to the required force that has to be exerted on the handrims to halt the wheelchair. The braking action has also been revealed to be an issue in terms of intuitiveness and multi-task procedure required to stop the wheelchair. Moreover, the lack of an active brake reduces the effectiveness of wheelchair handling during the downhill. Indeed, unlike the other solutions, rear add-on devices don't

provide any braking assistance during the downhill. This aspect has been highlighted as a safety concern by the users who tested the devices [9].

The introduction of an active braking system in the rear add-on devices could make them safer and would increase wheelchair handling. For this reason, the following work aims to investigate the possibility of implementing servo braking in rear-mounted devices and analyse the effectiveness of the braking force.

2 Wheelchair and add-on models

A dynamic multibody model of a wheelchair was developed and implemented in Simulink Simscape multibody environment, as in Fig. 1a. A standard reference wheelchair (14 kg and 24 inches wheels diameter) and a multibody dummy 50th percentile Italian male were considered. The contact between tyres and ground was modelled as a visco-elastic contact model. The stiffness and damping coefficients of the tyres were defined [13]. The friction between the ground and the wheels was modelled as Coulomb and rolling friction [14]. The attached wheel was assumed as an omni wheel, hence the tangential friction force was modelled only in the rolling direction (i.e., orthogonal to the wheel axis). In the wheel axis direction, both friction force and rolling resistance were considered negligible. Table 1 shows the coefficients used for the wheelchair tyres and the add-on tyre contact models. The add-on influences the dynamics of the system pushing the wheelchair in the longitudinal direction. A parametric simplified model of an add-on device has been implemented.

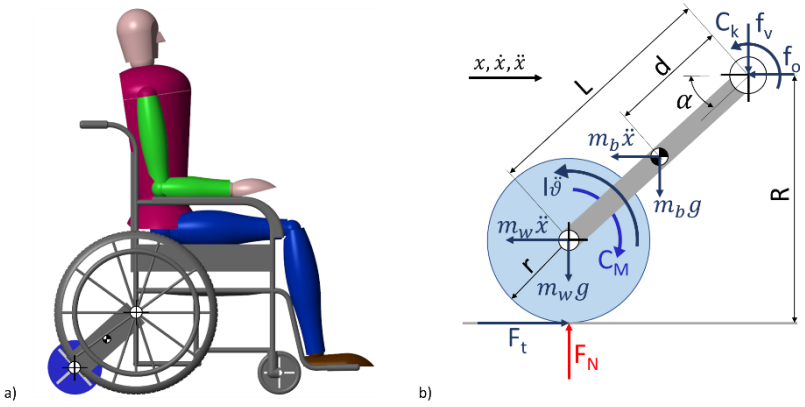

Fig. 1. (a) Multibody model of wheelchair, dummy, and add-on; (b) PAD free body diagram

The device model has been parametrized as a function of its geometrical parameters (d, L, r, R, α); Fig. 1b shows the PAD free body diagram. In the multibody model, the add-on has been attached at the wheels' axis through a joint as depicted in Fig. 1a.

Table 1. Friction, stiffness, and damping coefficient of the contact model

Tyre contact and friction model		
Stiffness	$6.8\ 10^4$	N/m
Damping	$1.0\ 10^4$	Ns/m
μ_s (static friction)	0.65	
μ_d (dynamic friction)	0.5	
f (rolling friction coeff.)	0.0099	

3 Tests and simulations

The rear-mounted wheel provides thrust to the wheelchair. In order to investigate the device's performance, various simulations have been carried out. Firstly, the driving mode has been considered and the dynamic of the system has been investigated as a function of the add-on's geometric parameter. Then, the braking mode has been studied and the forces that act on the system have been analysed. Considering the results obtained in the two different cases, a deeper evaluation of the effect of the braking torque and a possible design solution have been examined.

3.1 Test 1: driving torque

To evaluate the maximum torque transmissible to the ground without slipping, the trend of the normal force (F_N) exerted by the device to the ground, as the driving torque (C_m) varies has been observed. The simulation has been performed with the devices hooked to the wheelchair's axle in steady-state conditions. Results for add-on geometrical parameters L=0.3 m and r=0.1 m are reported. Eq. (1) shows the relation between the normal force and the driving torque:

$$F_N = \left(m_w + m_b \cdot \frac{d}{L}\right) \cdot g - \left(\frac{I \cdot \ddot{\theta}}{r} + \left(m_w + m_b \cdot \frac{d}{L}\right) \cdot \ddot{x}\right) \cdot tg(\alpha) + \\ + C_m \cdot \left(\frac{tg(\alpha)}{r} + \frac{1}{L \cdot \cos(\alpha)}\right) + \frac{C_k}{L \cdot \cos(\alpha)} \quad (1)$$

where geometric parameters (d, L, r, R, α) are depicted in Fig. 1b, m_w and m_b are the masses of the add-on's wheel and the add-on's body respectively. I is the moment of inertia of the wheel. $\ddot{\theta}$ and $\ddot{x}$ are the angular acceleration and linear acceleration of the add-on's wheel respectively. C_k is an eventual additional preload torque acting on the device. The contributions of the inertial force and torque are negligible because the test has been performed in steady-state conditions. No additional torque has been considered, hence, Eq. (1) could be rearranged as a function of two coefficients, A and K:

$$F_N = A + C_m \cdot K \quad (2)$$

Normal force (red line) and driving torque (blue line) tendency during a startup simulation are shown in Fig. 2a. According to Eq. (2), the result shows a linear trend of the normal force as the driving torque varies, as represented in Fig. 2b. The initial offset of

the plots is represented by A. The normal force linearly increases with the increase of the driving torque. The slope K of the curve is only influenced by the add-on geometrical parameters. With the geometric parameters chosen for the driving test, K is 13.4 m^{-1}. In Fig. 2b the black dotted line represents the slipping limit computed according to the static friction coefficient and the wheel's radius, as in Eq. (3):

$$F_{N_{lim}} = C_m/(\mu_s \cdot r). \tag{3}$$

The angular coefficient of the slipping limit line is 15.4 m^{-1}. Hence, the two lines are incident, and the crossing point is given as follow:

$$C_{m_{lim}} = \left(\frac{\left(m_w + m_b \cdot \frac{d}{L}\right)}{\frac{1}{(\mu_s \cdot r)} - \frac{tg(\alpha)}{r} + \frac{1}{L \cdot \cos(\alpha)}} \right) \tag{4}$$

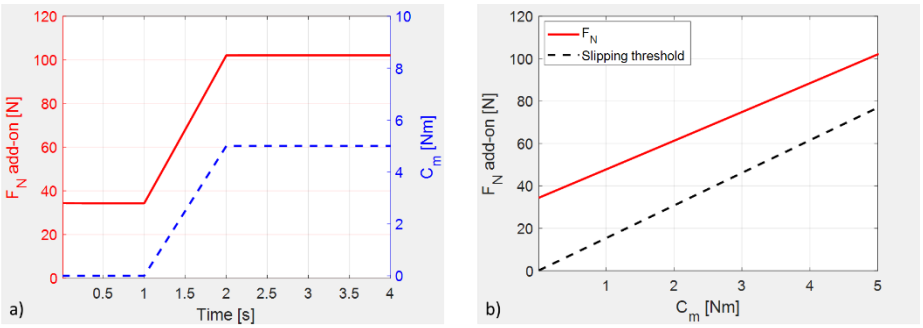

Fig. 2. (a) Normal force F_N and the driving torque C_m; (b) Relation between F_N and C_m.

3.2 Test 2: braking torque

In order to simulate a braking effect on the system, the direction of the torque delivered by the motor was inverted. Considering a negative C_m exerted by the wheel, the relation between F_N and C_m expressed in Eq. (1) remains unchanged. For the sake of clarity from now on the braking torque is called C_b and corresponds to $-C_m$.

Hence, when the braking torque increases, the normal force decreases with a slope that changes when the slipping threshold is achieved, as shown in Fig. 3a and 3b, without any additional torque C_k. When the wheel starts to slip, inertial effects of the add-on wheel change the normal force trend.

As it can be deduced by the results of the previous section, the normal force during the braking action is not sufficient to generate an effective braking force. Therefore, an additional preload torque C_k was applied between the wheelchair and the frame of the device. Four tests have been performed increasing the maximum braking torque by 2 Nm steps, setting the initial torque equal to 1 Nm and the initial speed equal to 8 km/h for each test.

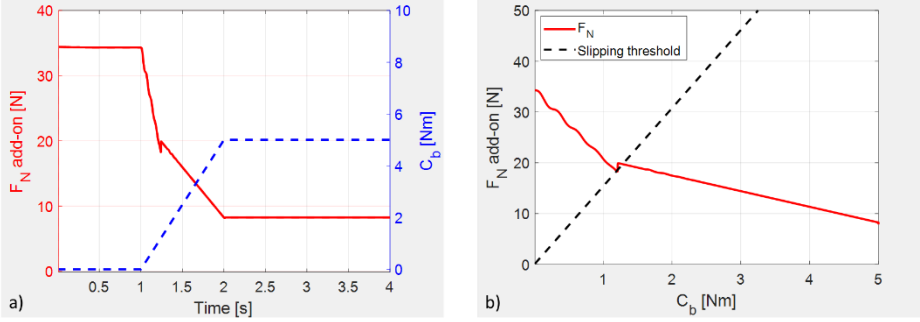

Fig. 3. (a) Normal force F_N and the braking torque C_b; (b) Relation between F_N and C_b.

During the tests, to simulate an instantaneous brake, the torque was increased from 0 to the set value in 0.1 s. To compare the results, the distance x_f and time t_f needed to stop the wheelchair have been measured. Aiming to ensure pure rolling condition, the minimum preload $C_{k_{min}}$ has been computed considering the wheel to ground dynamic friction coefficient. Hence, if the wheel started to slide, the normal force would be sufficient to restore the adhesion condition. In Table 2, the values measured in the four tests have been reported. Enhancing the preload, the maximum transmissible torque increases. The normal force and the stopping distance are plotted in Fig. 4.

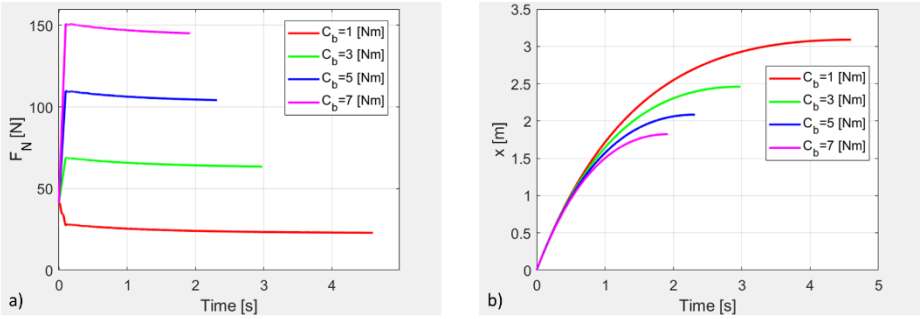

Fig. 4. Normal force (a) and stopping distances (b) for different braking torques.

As shown in Fig 4, in the test T4 t_f and x_f are 1.9 s and 1.8 m respectively. Whereas, in the test T1 conducted without preload and with a braking torque equal to 1 Nm, t_f and x_f are almost twice. Hence results show that the introduction of a mounting preload would enhance the braking effectiveness.

Table 2. Stopping time and distances evaluated introducing the preload

Test	C_b [Nm]	$C_{k_{min}}$ [Nm]	t_f [s]	x_f [m]
T1	1	0	4.7	3.1
T2	3	15	3	2.5
T3	5	30	2.3	2.1
T4	7	44	1.9	1.8

4 Discussion and conclusions

In this paper, the dynamic of a rear add-on device in driving and braking conditions has been analysed. The simulation results suggest that the normal force has a linear dependency on the driving torque represented by the *K* factor, whose value depends only on the geometric configuration. Increasing the radius or the length of the rear-mounted device, the *K* factor decrease. Generally, the maximum transmissible torque during the pushing mode is sufficient to ensure an effective thrust. Then, the effectiveness of the braking action has been investigated. Results show that the normal force exceeds the slipping threshold. The normal force decreases as the braking torque act due to the negative contribution of the torque and inertia.

Considering the results obtained in the two different dynamic configurations, a preload torque C_k has been added to guarantee effective braking. Four tests have been performed introducing the maximum admissible braking torque accordingly to the slipping threshold. The presence of the preload positively affects the normal force ensuring pure rolling also during the braking phase. However, the constant presence of a preload would inevitably increase the tire wear, causing a shortening of the useful life of the device's wheel. For this reason, would be suggested to introduce C_k only during the braking phase. The effectiveness of a braking force is quite evident by looking at the braking distances and times reported in Table 2. Moreover, the servo braking system would reduce the physical effort of the user, as the device assists the user to perform part of the braking action.

Acknowledgement

This research was partially conducted within the project "Advanced Light Body Assistants - Sistema avanzato leggero per l'assistenza a persone diversamente abili"- P.O.R. FESR 2014/2020 - Azione I.lb.2.2 Bando Pi.Te.F

References

[1] P. Cavallone, A. Botta, E. Bonisoli, and G. Quaglia, "Preliminary Experimental Test of a Cable-Driven Wheelchair in Different Configurations," *Mech. Mach. Sci.*, vol. 108 MMS, pp. 166–173, 2022, doi: 10.1007/978-3-030-87383-7_18.

[2] S. D. Algood, R. A. Cooper, S. G. Fitzgerald, R. Cooper, and M. L. Boninger, "Effect of a pushrim-activated power-assist wheelchair on the functional capabilities of persons with tetraplegia," *Arch. Phys. Med. Rehabil.*, vol. 86, no. 3, pp. 380–386, 2005, doi: 10.1016/j.apmr.2004.05.017.

[3] R. A. Cooper *et al.*, "Evaluation of a pushrim-activated, power-assisted wheelchair," *Arch. Phys. Med. Rehabil.*, vol. 82, no. 5, pp. 702–708, 2001, doi: 10.1053/apmr.2001.20836.

[4] S. D. Algood, R. A. Cooper, S. G. Fitzgerald, R. Cooper, and M. L. Boninger, "Impact of a pushrim-activated power-assisted wheelchair on the metabolic demands, stroke frequency, and range of motion among subjects with tetraplegia," *Arch. Phys. Med.*

Rehabil., vol. 85, no. 11, pp. 1865–1871, 2004, doi: 10.1016/j.apmr.2004.04.043.

[5] C. E. Levy, M. P. Buman, J. W. Chow, M. D. Tillman, K. A. Fournier, and P. Giacobbi Jr, "Use of Power Assist-Wheels Results in Increased Distance Traveled Compared to Conventional Manual Wheeling," *Phys. Med. Rehabil. Serv.*, vol. 89, no. 8, pp. 625–634, 2010, doi: 10.1097/PHM.0b013e3181e72286.

[6] M. Khalili, A. Eugenio, A. Wood, M. Van der Loos, W. Ben Mortenson, and J. Borisoff, "Perceptions of power-assist devices: interviews with manual wheelchair users," *Disabil. Rehabil. Assist. Technol.*, vol. 0, no. 0, pp. 1–11, 2021, doi: 10.1080/17483107.2021.1906963.

[7] M. Khalili, G. Kryt, W. Ben Mortenson, H. F. M. Van der Loos, and J. Borisoff, "Comparison of manual wheelchair and pushrim-activated power-assisted wheelchair propulsion characteristics during common over-ground maneuvers," *Sensors*, vol. 21, no. 21, Nov. 2021, doi: 10.3390/S21217008.

[8] E. W. Flockhart, W. C. Miller, J. A. Campbell, J. L. Mattie, and J. F. Borisoff, "Evaluation of two power assist systems for manual wheelchairs for usability, performance and mobility: a pilot study," 2021, doi: 10.1080/17483107.2021.2001063.

[9] B. Sawatzky, W. Ben Mortenson, and S. Wong, "Learning to use a rear-mounted power assist for manual wheelchairs," *Disabil. Rehabil. Assist. Technol.*, vol. 13, no. 8, pp. 772–776, 2017, doi: 10.1080/17483107.2017.1375562.

[10] M. G. M. Kloosterman, J. H. Buurke, L. Schaake, L. H. V. Van Der Woude, and J. S. Rietman, "Exploration of shoulder load during hand-rim wheelchair start-up with and without power-assisted propulsion in experienced wheelchair users," *Clin. Biomech.*, vol. 34, pp. 1–6, 2016, doi: 10.1016/j.clinbiomech.2016.02.016.

[11] R. A. Cooper *et al.*, "Performance assessment of a pushrim-activated power-assisted wheelchair control system," *IEEE Trans. Control Syst. Technol.*, vol. 10, no. 1, pp. 121–126, 2002, doi: 10.1109/87.974345.

[12] K. L. Best, R. L. Kirby, C. Smith, and D. A. Macleod, "Comparison between performance with a pushrim-activated power-assisted wheelchair and a manual wheelchair on the Wheelchair Skills Test,", vol. 28, no. 4, pp. 213–220, Feb. 2009, doi: 10.1080/09638280500158448.

[13] J. Gordon, J. J. Kaualarich, and J. G. Thacker, "Tests of two new polyurethane foam wheelchair tires," *J. Rehabil. Res. Dev.*, vol. 26, no. 1, pp. 33–46, 1989.

[14] M. D. Hoffman, G. Y. Millet, A. Z. Hoch, and R. B. Candau, "Assessment of Wheelchair Drag Resistance Using a Coasting Deceleration Technique," *Am. J. Phys. Med. Rehabil.*, vol. 82, no. 11, pp. 880–889, 2003, doi: 10.1097/01.PHM.0000091980.91666.58.